Nanoscale Advances

ROYAL SOCIETY OF CHEMISTRY

REVIEW

View Article Online
View Journal | View Issue

Cite this: *Nanoscale Adv.*, 2020, **2**, 5516

Overview of transition metal-based composite materials for supercapacitor electrodes

Mingjin Cui and Xiangkang Meng *

Supercapacitors (SCs) can bridge the gap between batteries and conventional capacitors, playing a critical role as an efficient electrochemical storage device in intermittent renewable energy sources. Transition metal-based electrode materials have been investigated extensively as a class of electrode materials for SC application, but they have some limitations due to the sluggish ion/electron diffusion and inferior electronic conductivity, restricting their electrochemical performances towards energy storage. Developing advanced transition metal-based electrode materials is crucial for high energy density along with high specific power and fast charging/discharging rates towards high performance SCs. In this review, we highlight the state-of-the-art of transition metal-based electrode materials (transition metal oxides and their composites, transition metal sulfides and their composites, and transition metal phosphides and their composites), focusing on specific morphologies, components, and power characteristics. We also provide future prospects for transition metal-based electrode materials for SCs and hope this review will shed light on the achievement of higher performance and hold great promise in vast applications for future energy storage and conversion.

Received 13th July 2020
Accepted 15th September 2020

DOI: 10.1039/d0na00573h

rsc.li/nanoscale-advances

1. Introduction

SCs are significantly competitive for harvesting applications in portable electronics, hybrid electric vehicles, and large industrial equipment energy storage because of their high power density (>10 kW kg^{-1}), rapid charge and discharge (a few seconds), high-prolonged cycle life (>100 times battery life) and service safety.[1–4] Owing to their merits relative to batteries, SCs fill the gap between batteries and conventional solid state and electrolytic capacitors, playing a critical role in the large-scale deployment of intermittent renewable energy sources.[5–8] Recently, transition metal-based electrode materials have been widely studied for achieving low-cost, fast charge–discharge processes, high powerful performance and long cycle life for SCs.[9–11] However, the main challenges for transition metal-based electrode materials are their low energy density, high internal resistance at the material interfaces, poor mechanical

National Laboratory of Solid State Microstructures, Collaborative Innovation Center of Advanced Microstructures, College of Engineering and Applied Sciences, Institute of Materials Engineering, Nanjing University, Jiangsu, 210093, P. R. China. E-mail: mengxk@nju.edu.cn

Mingjin Cui is a PhD candidate at the College of Engineering and Applied Science, Nanjing University, P. R. China. She received her B.E. degree from Northeast Forestry University in 2011. Her research interest focuses on nanomanufacturing for energy storage devices.

Dr Xiangkang Meng is a professor of Materials Science at the National Laboratory of Solid-State Microstructures, Nanjing University. His research is concerned with the preparation, microstructure and mechanical properties of nano-metallic materials, which includes controllable fabrication of metallic nanoparticles, microstructure evolution of metallic films, size effects on the mechanical behavior of metallic films, and thermodynamic and molecular dynamic models for the size-dependent behavior of metallic nanowires, nanorods, and nanoparticles.

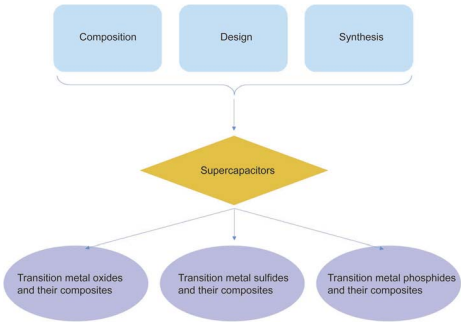

Scheme 1 Transition metal-based electrode materials focusing on their composition, design, and synthesis.

durability, and controversial environmental concerns.[12–14] Notable improvement in the performance of transition metal-based oxides, sulfides and phosphides has been demonstrated in recent years due to the understanding of their charge storage mechanisms, discovery of advanced nanostructured electrode materials as well as the design of new hybrid systems combining faradaic and capacitive electrodes.[15–17] Many strategies were proposed to boost the performance of transition metal-based electrode materials: firstly, considerable research has been developed to design and synthesize nanostructured transition metal-based electrode materials with large specific surface areas and porous structures, which could expose more electroactive sites for the redox reactions, and provide large contact area between the electrodes and electrolyte.[18–20] Hierarchically porous nanostructures provide not only more active sites but also fast electrode/electrolyte interaction and ion transport/electron interchange, and thus lead to enhancement in power density and rate capability.[21,22] Furthermore, the synergistic effect between multi-valence metal cations was explored based on the understanding of the mechanism of charge storage. The compositional synergy of the composite can afford facile ion and charge transfer in the electrode, which assures richer redox reactions.[22–25] In addition, tremendous efforts have been made to design various ternary and quaternary transition metal-based electrodes, which have been shown to possess distinguished advantages such as metallic conductivity, richer redox reaction sites, and electrochemical stability compared with monometallic oxides.[26–30] Finally, powdered electrode materials are mechanically unstable and their conductivity is typically too low for rapid charging–discharging. Due to the short diffusion distance of electrolytes into electrodes, only the surface of the material effectively contributes to the total capacitance. Designing additive-free electrode materials, directly growing on conducting porous substrates (*e.g.* foam Ni), not only improves the conductivity and richness in

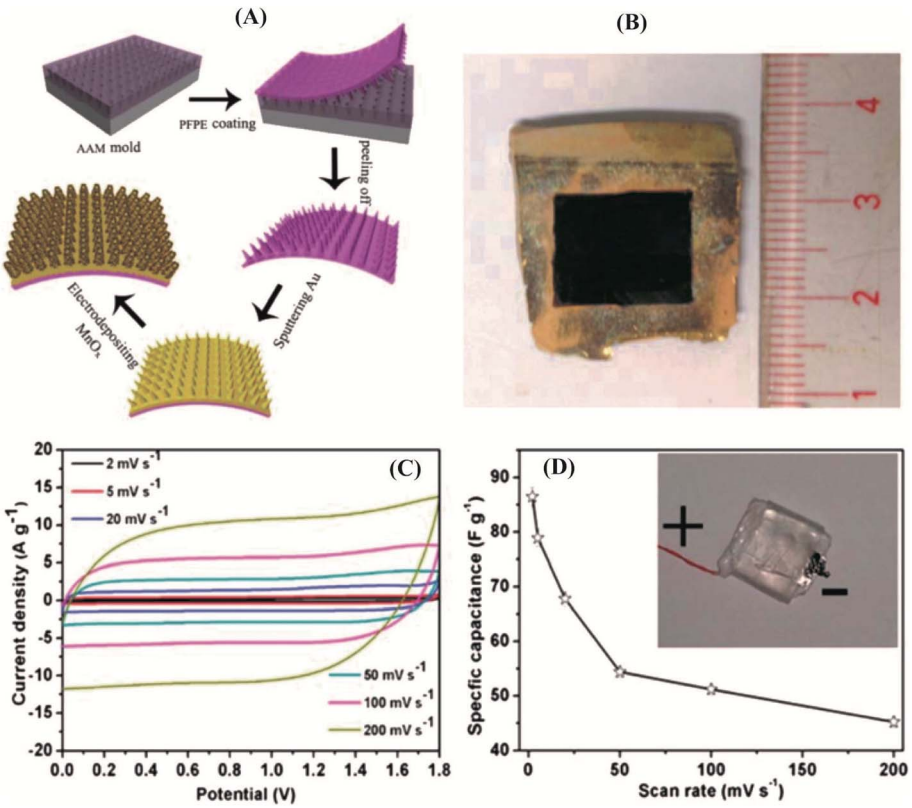

Fig. 1 Fabrication of the 3D metal/oxide nanocone array electrode. (A) Schematic diagram of the fabrication process of the 3D flexible nanocone array electrode. (B) Optical image of an as-prepared 3D Au/MnO_x nanocone array electrode. Performance testing of a full SC consisting of the 3D Au/MnO_x nanocone array positive electrode and a CCG negative electrode. (C) CV curves of the full SC at various scan rates in 1 M Na_2SO_4. (D) Corresponding specific capacitance as a function of scan rates.[64]

accessible electroactive sites, but also contributes to the stability of the nanostructure.[31–34]

In the present paper, we give a mini-review of the state-of-the-art of transition metal-based electrode materials, such as transition metal oxides, hydroxides and their composites, transition metal sulfides and their composites, and transition metal phosphides and their composites, focusing on their design and synthesis (Scheme 1). More importantly, their electrochemical performances are also discussed by virtue of the effects of morphology, structure, and composition of transition metal-based materials, and the current challenges and prospective analysis are outlined for transition metal-based electrode materials used in SCs.

2. Transition metal oxides as electrode materials

Transition metal oxides hold promise for achieving high levels of energy storage, especially for SC electrode materials, featuring low cost, environmentally benign nature, and high theoretical capacitance.[19,35–41] The strategies in building the structure of transition metal oxides such as designing particular nanoarchitectures, combining oxide composites with multiple oxidation states, and multiple transition metal oxides, demonstrate transition metal oxides as an advanced electrode material for high-energy and high-power density electrochemical storage devices.

2.1. Transition metal oxides (M_xO_y) and their composites

Pseudo-capacitive oxides of transition metals (Ni,[42,43] Co,[44,45] Fe,[18,46–48] Mn,[49,50] *etc.*) are widely explored because of their high theoretical capacitances, low cost, and reversible faradaic redox reactions, leading to higher specific capacitances compared to carbonaceous materials based on an electrical double-layer charge storage mechanism.[5,51–55] Although transition metal oxides exhibit good electrochemical activities, their conductivity is typically low resulting in an obvious decrease in rate capability. Thus, their real practical capacitances are far from theoretical expectations because of their intrinsically low electronic and ionic conductivities.[56] Recently, considerable strategies have been explored to tune their nanostructures, such as introducing transition metal oxides into a conducting substrate,[51,57] doping of the metals to increase the conductivity and redox activity,[27,58] and combining oxide composites with multiple oxidation states.[38,59]

Combining oxide composites featuring multiple oxidation states with a conducting substrate to enhance electrical conductivity has been widely used as the most efficient approach to improve energy densities. Taking MnO_x-based composites as an example, the pseudo-capacitance of MnO_2 originates from the fast, reversible successive surface redox reactions between Mn^{3+} and Mn^{4+}.[60–63] Thus, the maximum and minimum values of the polarization potential are controlled by the irreversible reactions of Mn^{4+} being oxidized to Mn^{7+} and Mn^{4+} being reduced to Mn^{2+}, respectively. Great progress has been made in MnO_x-based composites; for example, Qiu *et al.* reported a hybrid 3D Au/MnO_x nanocone array electrode using imprinting and soft-printing technologies[64] (Fig. 1). The array exhibits advanced advantages, including a number of active sites, high electrode surface area, and ease of electrolyte permeation. Most importantly, the Au/MnO_x composite contains complicated phases (Mn_3O_4, MnOOH), which promote proton migration in manganese oxide by hopping between the H_2O and OH sites, improving the ion conductivity. The hybrid Au/MnO_x electrode achieved remarkable electrochemical performance, a specific mass capacitance of 840.3 F g^{-1} at a current density of 2 A g^{-1}, which is superior to those of most reported SCs.

To enhance the ultrafast electron and ion transport at high mass loadings of MnO_2, Liu *et al.* designed porous carbon fiber (PCF) with uniform mesopores of 11.7 nm as a lightweight, flexible, binder-free, and conductive-additive-free support for ultrathin MnO_2.[65] PCFs with uniform mesopores are superior carbon supports for addressing the high mass loading and fast charge transport. For MnO_2-coated PCFs with mass loadings approaching 7 mg cm^{-2}, the gravimetric and areal capacitances of MnO_2 (~50% of total mass) reach 1148 F g^{-1}, which

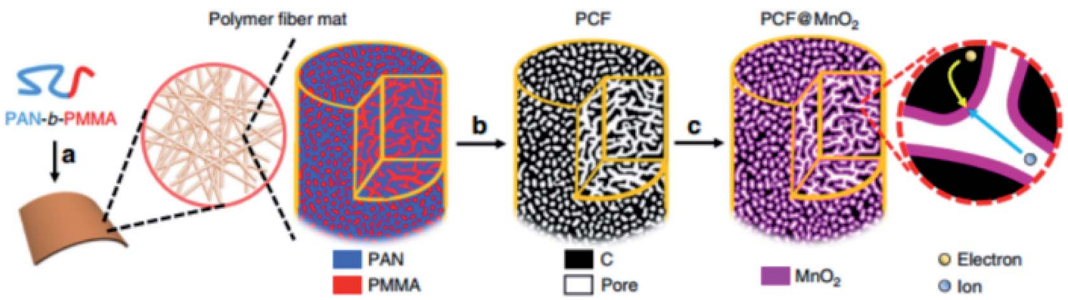

Fig. 2 Schematic illustration of the synthesis of PCF and PCF@MnO_2. (a) PAN-*b*-PMMA block copolymer is spun into a polymer fiber mat. (Magnified view) PAN (blue) and PMMA (red) in the block copolymer fiber microphase separate into a bicontinuous network structure. *Via* thermal oxidation, PAN is crosslinked to ensure a high yield of conductive carbon network. (b) Upon pyrolysis, the polymer fibers are converted to porous carbon fibers (PCFs, black) with continuous and uniform mesopores (white channels), which afford high loadings of transition metal oxides. (c) The PCFs are loaded with MnO_2 (magenta) to become PCF@MnO_2 through a solution-based redox deposition reaction. (Magnified view) The continuous carbon fiber matrix and the partially filled mesoporous channels provide effective expressways for electron conduction and ion diffusion, respectively.[65]

outperform most other MnO_2-based electrodes at similar loadings (Fig. 2).

Although a huge number of research studies have been devoted to hybrid SC electrode materials, achieving nanoarchitectures and composites with multiple oxidation states for advanced electrode materials is a daunting task. Recently, our group developed a novel Mn_3O_4/MnO_2 hierarchical nanoarchitecture/N-doped graphene (NG) composite as an advanced SC electrode material[60] (Fig. 3a). The Mn_3O_4/MnO_2 particles consist of monolayer standing MnO_2-nanosheet covered Mn_3O_4 octahedra; they are closely anchored, well dispersed in the NG networks. The 3D conductive network of NG providing an open

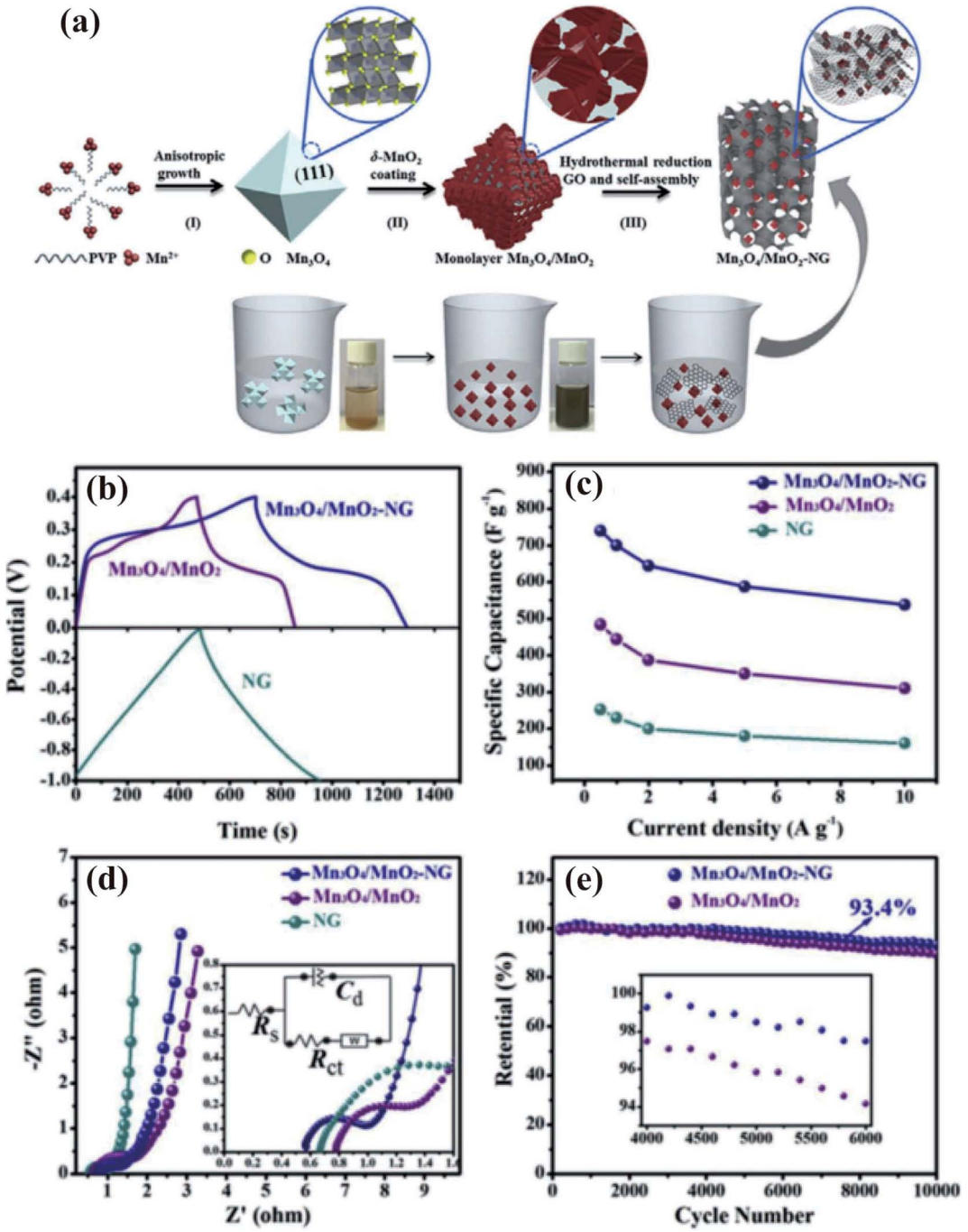

Fig. 3 (a) Schematic illustration of the synthetic process of Mn_3O_4/MnO_2-NG and the specific nanostructure of Mn_3O_4 octahedra, Mn_3O_4/MnO_2 particles, and Mn_3O_4/MnO_2-NG. Digital photographs of glass bottles with bare Mn_3O_4 and Mn_3O_4/MnO_2 suspensions are also presented. (b) GCD curves of the Mn_3O_4/MnO_2-NG, Mn_3O_4/MnO_2, and pure NG electrodes. (c) The corresponding specific capacitances of the three types of electrodes as a function of current density. (d) EIS curves with the insets showing magnified semicircles and electrochemical equivalent circuits, and (e) the capacitance retention of the Mn_3O_4/MnO_2-NG and Mn_3O_4/MnO_2 electrodes over 10 000 cycles at 10 A g^{-1} with the inset showing the 4000th to 6000th cycle.[60]

pathway for electron/ion transport together with closely touching Mn_3O_4/MnO_2 assures both enhanced conductivity and strong component synergy, thus promoting the electrode reaction kinetics. This work is an advancement in the particularly important research fields of energy materials for high performance SCs, the as-prepared Mn_3O_4/MnO_2-NG exhibiting a high specific capacitance of 739 F g^{-1} at 0.5 A g^{-1}, excellent rate capability, and 93.4% capacitance retention over 10 000 cycles (Fig. 3b–e).

2.2. Ternary transition metal oxides ($M_xN_yO_z$) and their composites

As mentioned above, although transition metal oxides exhibit good electrochemical activities, they demonstrate inferior electrical conductivity and low rate capability. As such, bimetallic oxides such as $M_xN_yO_z$ with M/N being Zn,[66,67] Ni,[68–70] Mn,[71] Co,[72–74] or Cu[75] possess high specific capacitances due to their better electrical conductivity and higher active redox sites, as well as mechanical and thermal stability compared to their corresponding single component counterparts. For example, $NiCo_2O_4$, which exhibits two orders of magnitude higher electrical conductivity[76] than nickel or cobalt oxides,[44] and iron oxides[46] provides excellent electrochemical performance, therefore Fe–Co oxide ($FeCo_2O_4$) should be an even better material since it offers richer redox reactions than the single components. Sethi M. *et al.* reported the facile solvothermal synthesis of a porous graphene–$NiFe_2O_4$ (PGNF) nanocomposite,[77] which displayed an impressive specific capacitance value of 1465.0 F g^{-1} at a scan rate of 5 mV s^{-1} along with a high capacitance retention of 94% after 10 000 discharge

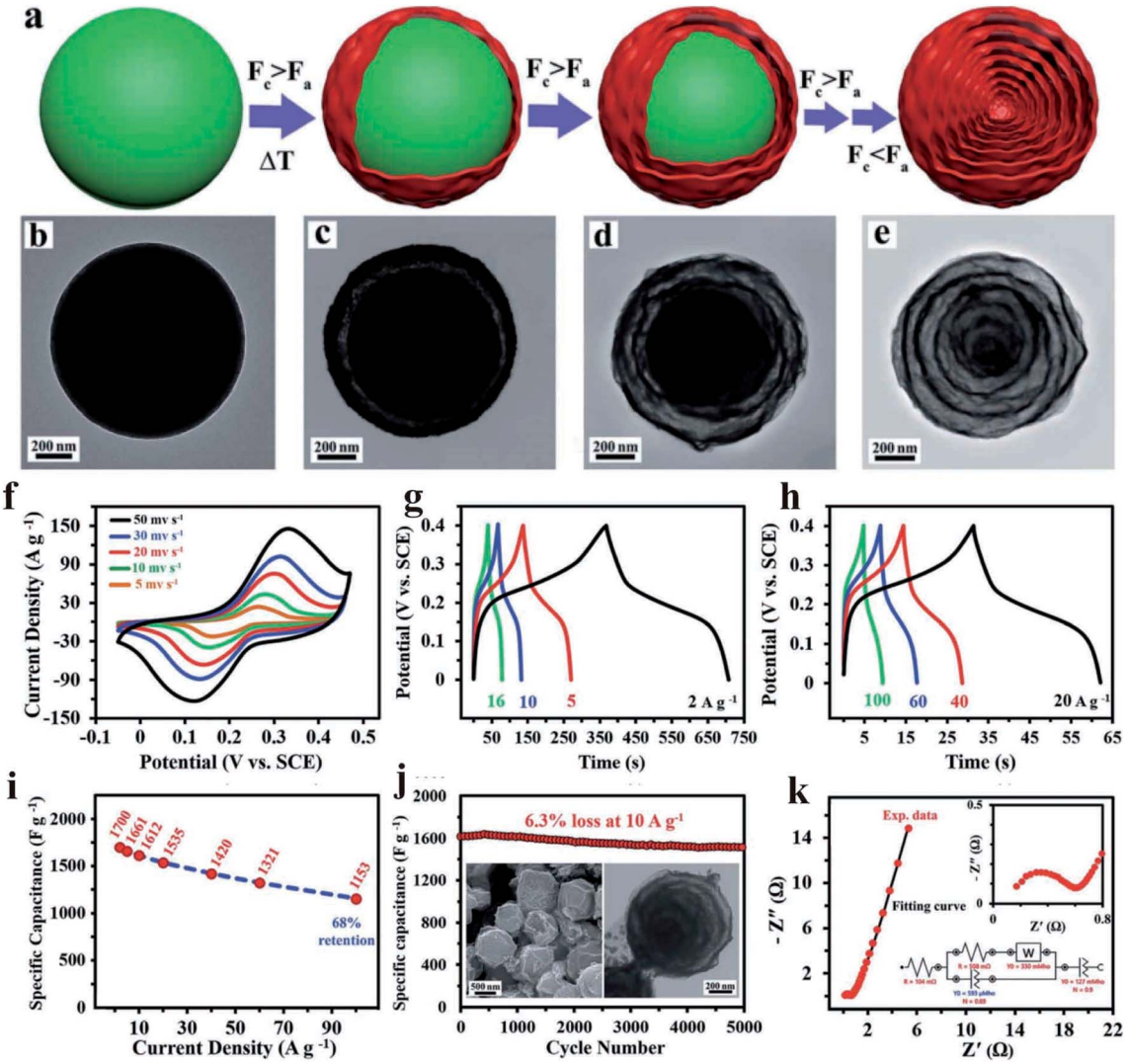

Fig. 4 (a) Schematic illustration of the onion-like structure formation process. TEM images of the (b) Cu–Co precursor and the obtained products after calcination of the precursors to different temperatures: (c) 350 °C, (d) 400 °C, (e) 500 °C. Evaluation of the electrochemical performance of the ON-CCO electrode in a three-electrode cell. (f) CV curves of the ON-CCO electrode at different scan rates. (g and h) CD curves of the ON-CCO electrode at various current densities. (i) Rate capability of the ON-CCO electrode. (j) Long-term cycling stability of the ON-CCO electrode at a current density of 10 A g^{-1}. Insets show the SEM and TEM images of the electrode after cycling. (k) Nyquist plot of the ON-CCO electrode with its equivalent circuit (inset) used to fit the experimental data.[79]

cycles. The excellent performance is attributed to the synergic effect between the porous graphene and bimetallic oxidation and connotes their robust application for supercapacitors. Zhu X. X. *et al.* fabricated the three-dimensional hierarchical self-supported $NiO/Co_3O_4@C/CoS_2$ hybrid electrode, in which NiO/Co_3O_4 nanosheets are *in situ* grown on a nickel foam substrate and combined with CoS_2 nanospheres through a carbon medium.[78] The porous structure of the $NiO/Co_3O_4@C$ nanosheets and CoS_2 nanospheres contributes to the high electrochemical performance. Most recently, Chu *et al.* reported phosphorus doped $NiCo_2O_4$ (P–NCO) featuring rich oxygen vacancies synthesized by a hydrothermal treatment, followed by phosphatization in a tube furnace.[9] The novel structure of $NiCo_2O_4$ (P–NCO) with greatly improved electrical conductivity shows an ultrahigh specific capacitance of 2747.8 F g^{-1} at 1 A g^{-1} and significant rate performance. Ensafi *et al.* synthesized onion-like nanoporous $CuCo_2O_4$ hollow spheres (ON-CCO) derived from bimetal–organic frameworks with a high surface area of 63 m^2 g^{-1} and more than six thin shells[79] (Fig. 4). The ON-CCO electrode presented the desired electrochemical performance with high reversibility, fast kinetics, low internal resistance, and an ultrahigh specific capacitance. Although binary transition metal oxides show higher energy density than monometallic oxides due to the higher capacity of binary transition metal oxides compared to monometallic oxides, transition metal oxides still suffer from the intrinsic drawback of poor conductivity, leading to low rate capabilities and power density.

3. Transition metal sulfides as electrode materials

Transition metal sulfides as a new class of pseudo-capacitive materials have been extensively studied because of their capabilities to provide high energy density.[10,11,15,80–83] Bimetallic

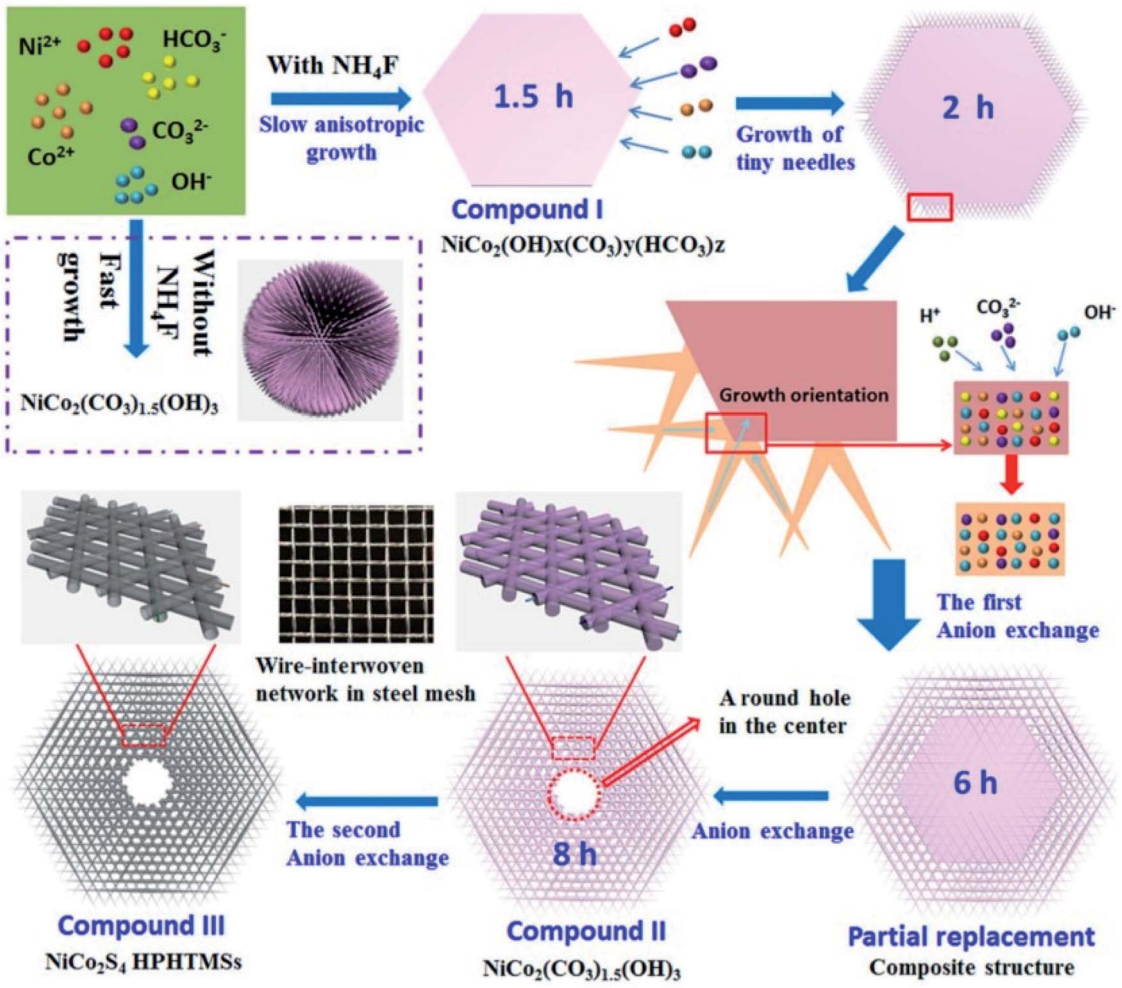

Fig. 5 Schematic illustrating the formation process of $NiCo_2S_4$ HPHTMSs constructed with well-interwoven NTs. In the presence of NH_4F, a slow anisotropic growth leads to compound I of composition $NiCo_2(OH)_x(CO_3)_y(HCO_3)_z$, while the product is already compound II of composition $NiCo_2(OH)_3(CO_3)_{1.5}$ after only 0.5 h and its morphology is spherical with a rough NW-covering without NH_4F. The nanostructure and composition change with time are presented in detail during the first ion-exchange process from compound I to compound II. The second anion-exchange results in the formation of compound III, $NiCo_2S_4$ HPHTMSs. The insets illustrate local magnifications of several interwoven NWs and sulfide NTs. A wire-interwoven network structure is also presented in a steel mesh with strong mechanical stability.[98]

sulfides show superior electrochemical characteristics over their oxide counterparts and exhibit enhanced electrical conductivity by two orders of magnitude and a greatly improved redox reaction.[3,11,12,41,84–87]

3.1. Binary transition metal sulfides ($M_xN_yS_z$)

Most binary metal sulfide nanostructures have been reconstructed from their corresponding metal oxide/hydroxide precursors by applying the hydrothermal method followed by an anion exchange, based on the mechanism of the Kirkendall effect that offers the potential growth of tunable morphologies, such as nanoparticles,[88,89] nanowires,[90,91] nanotubes,[92–94] and nanosheets.[95,96] Kirkendall effect is a well-known phenomenon resulting from the mutual diffusion process of chemical constituents through an interface, featuring the difference in the atomic diffusion coefficients of chemical constituents. Because of the unbalanced diffusion rates between the two chemical constituents, vacancies will be introduced near the interface of the faster diffusing chemical constituent, leading to a change in the position of the initial interface during the diffusion process. Vacancies gather together gradually to form cavities and finally evolve into a hollow structure.[97] Liu, T *et al.* reported NiCoS nanosheet arrays on carbon cloth as supercapacitor electrodes. The unique structure possessed abundant accessible active sites, and hence presented enhanced electrochemical performance.

In our previous work, we reported complex hierarchical structures by achieving novel hierarchically porous hexagonal micro-sheets constructed with well-interwoven nanotube networks using a controllable top-down, two-step anion-exchange technique[98] (Fig. 5). We applied a first anion-exchange step to achieve nanowire woven hexagons with uniform distribution, followed by the transformation of the nanowires to MCo_2S_4 nanotubes *via* a second anion-exchange process. The formation mechanism of the unique nanowire woven hexagonal architecture, ion-induced anisotropic growth and time-dependent anion-exchange reaction kinetics were investigated in depth. We also confirmed that the two-step anion-exchange method is a powerful and general method to synthesize other MCo_2S_4 with a nanotube-interwoven three-dimensional porous architecture. Owing to the well-defined morphology, large porosity, and low resistance, the $NiCo_2S_4$ electrode exhibits a higher capacitance of 1780 F g^{-1} at 1 A g^{-1} and superior rate capability compared to most reported $NiCo_2S_4$ nanostructures with different morphologies as well as 92.4% capacity retention after 10 000 charge–discharge cycles. An asymmetric solid state SC using $NiCo_2S_4$ as the positive electrode and N-doped graphene film as the negative electrode achieves outstanding cycle ability and higher energy density than similar devices.

Based on the Kirkendall effect, Yang *et al.* reported a hybrid architecture of edge site-enriched nickel–cobalt sulfide (Ni–Co–S) nanoparticles supported on graphene frameworks *via* an *in situ* chemical conversion method[99] (Fig. 6). The edge site-enriched nanostructure was fabricated by an etching-like effort of the S^{2-} ions by a Kirkendall effect-involved anion exchange reaction. The as-prepared Ni–Co–S/G hybrid electrodes possess a high specific capacitance of 1492 F g^{-1} at the current density of 1 A g^{-1}, superior rate capability of 96% when the current density is increased to 50 A g^{-1}, and excellent electrochemical stabilities. Furthermore, a two-electrode asymmetric SC made of the Ni–Co–S/G hybrids and porous carbon nanosheets shows a high energy density and power density, indicative of their potential as a promising candidate material for high-performance SCs. Collectively, these results demonstrate the great potential of this anion-exchange technique during the Kirkendall process in engineering the structures of nanoscale electrode materials for enhanced SC performance. However, the Kirkendall process is lack of the in-depth investigation. For

Fig. 6 Schematic illustrations of the *in situ* formation of the integrated edge site-enriched Ni–Co–S/G hybrid architectures (Strategy I), fabricated by the Kirkendall effect-involved anion exchange reaction of the NiCo-precursor on graphene with abundant S^{2-} ions derived from TAA. The B–Ni–Co–S/G hybrids were directly fabricated *via* a one-step hydrothermal method (Strategy II).[99]

example, the difference of the atomic diffusion coefficients of chemical constituents. Theoretical analysis by atomistic simulation studies should be investigated. We believe that the current and future studies could significantly broaden the application of the Kirkendall effect in the rational design of nanoscale structures, produce practically important electrode materials with enhanced activity and stability, and thus impact broad areas of application such as energy conversion and storage.

3.2. Binary transition metal sulfide composites

Binary transition metal sulfide composites are composed of binary transition metal sulfides with oxides,[100] hydroxides,[101] sulfides,[102–104] *etc.* The oxides, hydroxides, and sulfides take place different electrochemical redox reactions, which enrich the species of electrochemical redox reactions for achieving higher capacity and rate performance. Recently, extensive efforts have been devoted to the synthesis of binary transition metal sulfide composites for electrochemical energy storage.[105] As a representative example, our group fabricated a multicomponent hierarchical zinc cobalt sulfide (ZCS) hollow nanotube array wrapped with interlaced ultrathin $Ni(OH)_2$ nanoflakes for high-performance electrodes.[106] The schematic is depicted in Fig. 7. ZCS exhibits a unique pentagonal cross-section and a rough surface that facilitates the deposition of $Ni(OH)_2$ interlaced nanoflakes with a thickness of 7.5 nm (wrapping the ZCS hollow nanotubes), while the tubes are separated well apart

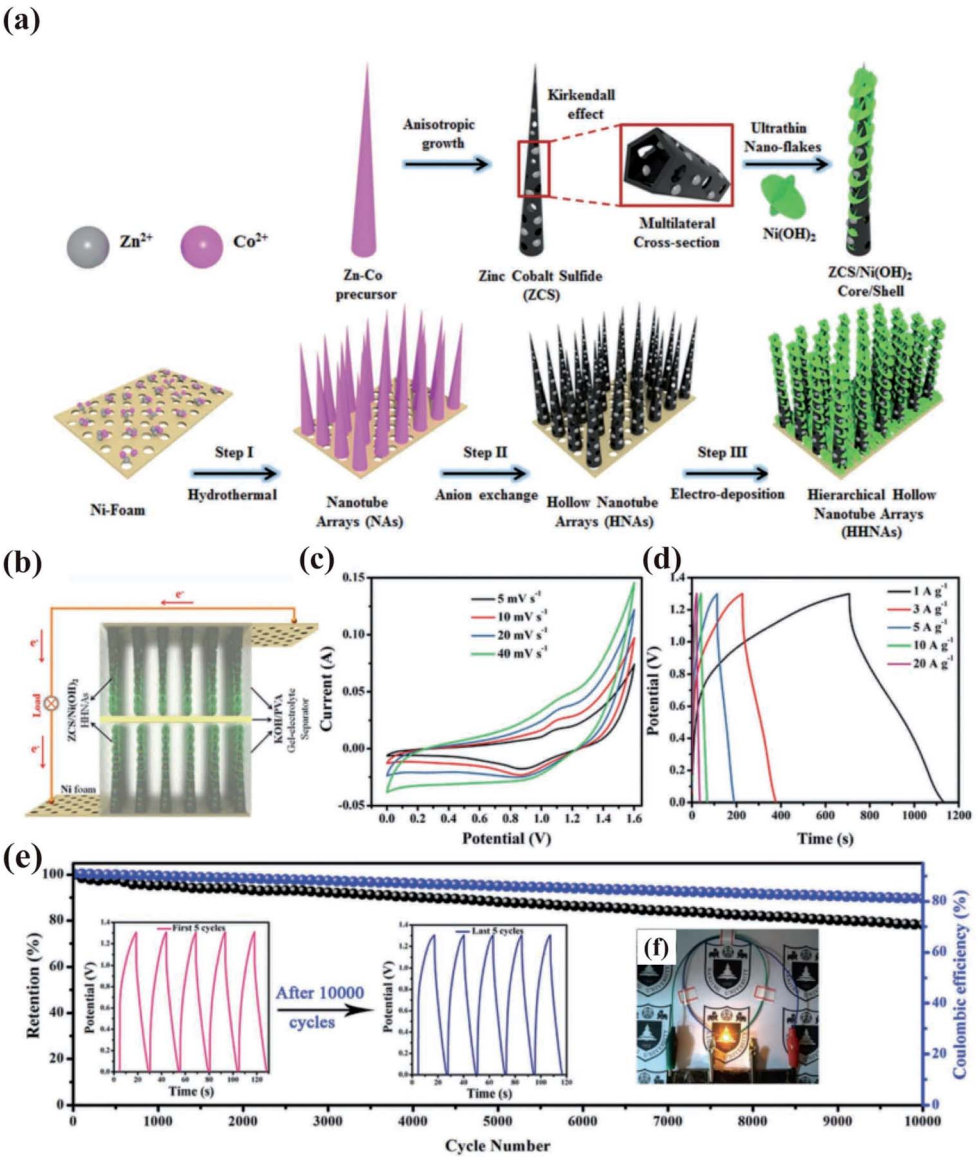

Fig. 7 (a) Schematic illustration of the fabrication of hollow ZCS NAs and ZCS/$Ni(OH)_2$ HHNA electrodes on Ni foam by a stepwise synthesis approach. Schematic illustration of (b) two hybrid electrodes assembled into symmetric SCs with a KOH–PVA gel–electrolyte separator, (c) CV curves of ZCS/$Ni(OH)_2$//ZCS/$Ni(OH)_2$ symmetric SCs at different scan rates, (d) GCD curves of hybrid symmetric SCs at different current densities, (e) cycling stability and coulombic efficiency of the hybrid symmetric SCs over 10 000 cycles with the inset showing the CD curves of the initial and last few cycles, and (f) an LED light illuminated with three symmetric SCs connected in series.[106]

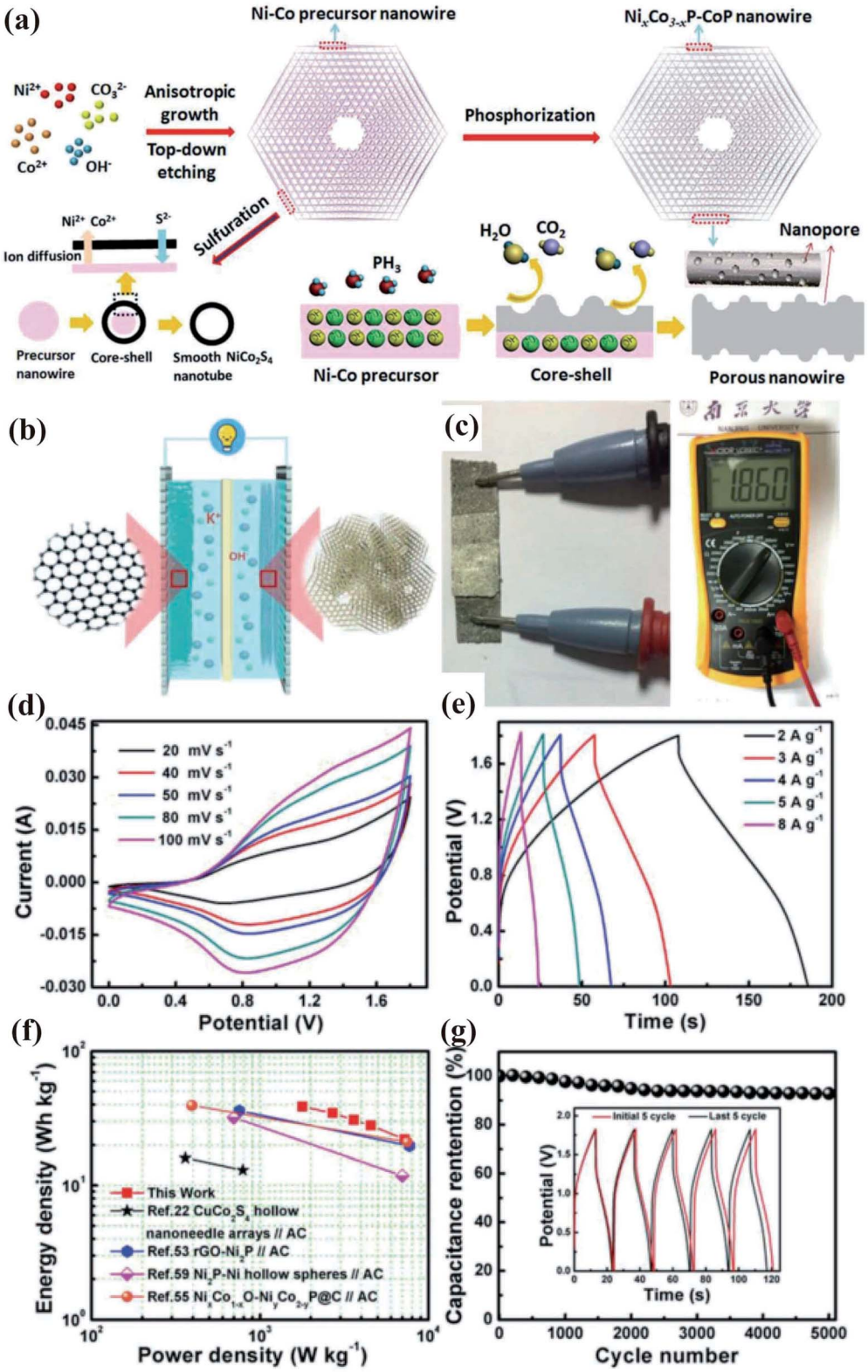

Fig. 8 (a) Schematic illustration of the formation process of PNWCHAs, the difference in the ion-exchange mechanisms results in different nanostructures. (b) Schematic illustrations of the assembled structure of a solid-state asymmetric SC with the PNWCHAs as the positive electrode and PNGF hydrogel film as the negative electrode. (c) The open-circuit voltage of the asymmetric SC. (d) CV curves at various scan rates and (e) GCD curves at different current densities of the NiCoP–CoP//PNGF ASC. (f) Ragone plots of the ASC in comparison to previous reports. (g) Charge–discharge cycling of the ASC at a high current density of 20 A g^{-1} with the inset showing the initial and last five cycles.[124]

and the interlaced flakes also maintain a certain distance between each other. The hierarchically porous ZCS/$Ni(OH)_2$ electrode demonstrates a high specific capacitance of 2156 F g^{-1} and excellent cycling stability with 94% retention over 3000 cycles. This is attributed to enhanced redox reactions, the direct growth of arrays on 3D porous foam for fast electron transport, and the increased availability of electrochemical active sites provided by the ultrathin $Ni(OH)_2$ flakes which also sustain the stability of the electrode by sacrificing themselves during long charge/discharge cycles. Additionally, symmetric SCs are assembled to achieve a high energy density of 74.93 W h kg^{-1} and exhibit superior cycling stability over 10 000 cycles.

4. Transition metal phosphides

Transition metal phosphides featuring metalloid characteristics and excellent electrical conductivity have shown excellent performances and great potential as a class of electrode materials for SC applications.[107–115] Compared with transition metal-based compounds such as oxides/hydroxides/sulfides, transition metal phosphides are kinetically favorable for fast electron transport[111,116–123] for achieving high power densities of SCs. In our previous work, we prepared novel phosphide composites ($Ni_xCo_{3-x}P_y$) with well-defined hexagonal thin-plate morphology and a hieratically porous but robust three dimensional network constructed by inter-welding porous nanowires, which are achieved by top–down etching, followed by phosphorylation treatment[124] (Fig. 8). Benefiting from the enhanced electron/ion transfer, increased availability of active sites/interfaces, rich mixed valences of metals and phosphorus, and strong componential synergy, the optimized NiCoP–CoP showed a specific capacitance reaching 1969 F g^{-1}, much higher than those of Ni–Co-based sulfides and other similar phosphides. When an asymmetric SC was fabricated, the NiCoP–CoP composite as the positive electrode exhibited a remarkable cycling stability with 93% retention after 5000 cycles at 8 A g^{-1}, which is mainly attributed to such an architecture that allowed strong mechanical stability and effectively buffered the strain/volume expansion during fast faradaic reactions. By taking advantage of state-of-the-art electrode materials and structural engineering, the proposed device will achieve higher performance and hold great promise in vast applications for future miniaturized electronics.

5. Summary and outlook

In this mini review, we summarized a number of research studies on transition metal-based materials, such as transition metal oxides and their composites, transition metal sulfides and their composites, and transition metal phosphides and their composites towards high performance SC application. Due to the high theoretical capacity, low cost and high activity, transition metal-based compounds are proposed as more promising candidates for electrochemical applications compared with carbon materials (active carbon, biochar, graphene, *etc.*). However, the wide application of transition metal oxides is limited by their intrinsically low electrical conductivity. To address the electrical conductivity problem, binary metal oxides and their composites were designed and synthesized by introducing a second transition metal and other compounds. Transition metal sulfides derived from oxides/hydroxides by sulfuration treatment are considered as promising electrodes for SCs. Furthermore, transition metal sulfides with rational design nanoarchitectures would effectively contribute to the large contact surface area of the electrode and electrolyte with sufficient electrochemical redox reactions, resulting in enhancement of the performance. Additionally, transition metal phosphides with high electronic conductivity as a new class of material were developed. Transition metal phosphides feature fast ion/electron diffusion/transport pathways to improve the thermodynamic and kinetic properties of electrochemical reactions for high performance. Although considerable efforts have been devoted to transition metal oxides/sulfides/phosphides and their composites, research on understanding the formation mechanism of their architecture and the reaction mechanism at the nanoscale or atomic scale is still a great challenge.

The future development trend of transition metal-based materials to meet the needs of increasing energy demand is proposed: firstly, an understanding of the formation mechanism of the nanoarchitecture and the charge storage mechanism is urgently required for the development of new types of electrode materials. For example, the charge storage mechanism of transition metal-based materials shows similar behavior to that of batteries rather than a pseudo-capacitive mechanism, however, it is usually considered as the pseudo-capacitive charge storage mechanism. Note that computational analysis and simulation methods in the atomic scale will be greatly helpful to comprehensively understand the formation mechanism of novel nanoarchitectures and the charge storage mechanism in depth. A good understanding of the mechanism can be a great guide to design next generation materials to increase the energy density of SC material systems. Secondly, the purpose of further development of SCs is for practical commercial applications instead of limiting to lab-scale investigation. However, it is still a great challenge to meet the requirement of high-energy storage for commercial applications. In addition, the accompanying important issues of large-scale fabrication by a facile synthesis method, cost-effectiveness, and environmental friendliness should be emphasized. Finally, developing and applying new machine-learning methods in material design would be an efficient strategy to achieve the screening of new and high performance capacitive-type electrode materials. Compared with machine-learning methods, traditional experiments or computational modelling is usually time-consuming and inefficient. Thus, building the structure–property relationship by machine-learning is necessary to provide insight into the parameters that affect the properties of materials, thereby making predictions for material discovery, rational design, and fabrication of the desired electrode materials.

Conflicts of interest

There are no conflicts to declare.

Acknowledgements

We acknowledge the financial support from the National Natural Science Foundation of China (Grant No. 51771090).

References

1 P. Simonand Y. Gogotsi, *Nat. Mater.*, 2008, **7**, 845–854.
2 T. Brezesinski, J. Wang, S. H. Tolbertand and B. Dunn, *Nat. Mater.*, 2010, **9**, 146–151.
3 L. Shen, L. Yu, H. B. Wu, X.-Y. Yu, X. Zhangand X. W. Lou, *Nat. Commun.*, 2015, **6**, 6694.
4 J. Wang, Y. Cuiand D. Wang, *Adv. Mater.*, 2019, **31**, 1801993.
5 J. Li, Z. Liu, Q. Zhang, Y. Cheng, B. Zhao, S. Dai, H.-H. Wu, K. Zhang, D. Ding, Y. Wu, M. Liuand M.-S. Wang, *Nano Energy*, 2019, **57**, 22–33.
6 C. Li, W. Wu, P. Wang, W. Zhou, J. Wang, Y. Chen, L. Fu, Y. Zhu, Y. Wuand W. Huang, *Adv. Sci.*, 2019, **6**, 1801665.
7 B. Kirubasankar, V. Murugadoss, J. Lin, T. Ding, M. Dong, H. Liu, J. Zhang, T. Li, N. Wang, Z. Guoand S. Angaiah, *Nanoscale*, 2018, **10**, 20414–20425.
8 P. Geng, S. Zheng, H. Tang, R. Zhu, L. Zhang, S. Cao, H. Xueand H. Pang, *Adv. Energy Mater.*, 2018, **8**, 1703259.
9 W. Chu, Z. Shi, Y. Hou, D. Ma, X. Bai, Y. Gaoand N. Yang, *ACS Appl. Mater. Interfaces*, 2020, **12**, 2763–2772.
10 S. Chandrasekaran, L. Yao, L. Deng, C. Bowen, Y. Zhang, S. Chen, Z. Lin, F. Pengand P. Zhang, *Chem. Soc. Rev.*, 2019, **48**, 4178–4280.
11 W. Liu, H. Niu, J. Yang, K. Cheng, K. Ye, K. Zhu, G. Wang, D. Caoand J. Yan, *Chem. Mater.*, 2018, **30**, 1055–1068.
12 C. Li, J. Balamurugan, D. C. Nguyen, N. H. Kimand J. H. Lee, *ACS Appl. Mater. Interfaces*, 2020, **12**, 21505–21514.
13 T. Wang, H. C. Chen, F. Yu, X. S. Zhaoand H. Wang, *Energy Storage Mater.*, 2019, **16**, 545–573.
14 J. Bai, B. Xi, H. Mao, Y. Lin, X. Ma, J. Fengand S. Xiong, *Adv. Mater.*, 2018, **30**, 1802310.
15 W. Xu, J. Lu, W. Huo, J. Li, X. Wang, C. Zhang, X. Guand C. Hu, *Nanoscale*, 2018, **10**, 14304–14313.
16 C. Chen, D. Yan, X. Luo, W. Gao, G. Huang, Z. Han, Y. Zengand Z. Zhu, *ACS Appl. Mater. Interfaces*, 2018, **10**, 4662–4671.
17 C. Zhao, C. Yu, M. Zhang, H. Huang, S. Li, X. Han, Z. Liu, J. Yang, W. Xiao, J. Liang, X. Sunand J. Qiu, *Adv. Energy Mater.*, 2017, **7**, 1602880.
18 K. A. Owusu, L. Qu, J. Li, Z. Wang, K. Zhao, C. Yang, K. M. Hercule, C. Lin, C. Shi, Q. Wei, L. Zhouand L. Mai, *Nat. Commun.*, 2017, **8**, 14264.
19 M. R. Lukatskaya, B. Dunnand Y. Gogotsi, *Nat. Commun.*, 2016, **7**, 12647.
20 W. Li, J. Liuand D. Zhao, *Nat. Rev. Mater.*, 2016, **1**, 16023.
21 X. Long, Z. Wang, S. Xiao, Y. Anand S. Yang, *Mater. Today*, 2016, **19**, 213–226.
22 B. Jiang, X. Ban, Q. Wang, K. Cheng, K. Zhu, K. Ye, G. Wang, D. Caoand J. Yan, *J. Mater. Chem. A*, 2019, **7**, 24374–24388.
23 X. Han, C. Yu, H. Huang, W. Guo, C. Zhao, H. Huang, S. Li, Z. Liu, X. Tan, Z. Gao, J. Yuand J. Qiu, *Nano Energy*, 2019, **62**, 136–143.
24 J. Hu, P. Yang, S. Wangand J. Shi, *ChemElectroChem*, 2019, **6**, 928–936.
25 W. Song, G. Wang, D. Zhao, Y. Zhou, Y. Ding, C. Tan, S. Tang, H. Dongand X. Meng, *ACS Appl. Mater. Interfaces*, 2019, **11**, 25271–25282.
26 S. Kumar, G. Saeed, N. H. Kimand J. H. Lee, *J. Mater. Chem. A*, 2018, **6**, 7182–7193.
27 Y. Yuan, W. Wang, J. Yang, H. Tang, Z. Ye, Y. Zengand J. Lu, *Langmuir*, 2017, **33**, 10446–10454.
28 M. Li, Y. Wang, H. Yangand P. K. Chu, *J. Mater. Chem. A*, 2017, **5**, 17312–17324.
29 M. A. Garakani, S. Abouali, Z.-L. Xu, J. Huang, J.-Q. Huangand J.-K. Kim, *J. Mater. Chem. A*, 2017, **5**, 3547–3557.
30 B. Y. Guan, A. Kushima, L. Yu, S. Li, J. Liand X. W. Lou, *Adv. Mater.*, 2017, **29**, 1605902.
31 B. Zhu, S. Tang, S. Vongehr, H. Xieand X. Meng, *ACS Appl. Mater. Interfaces*, 2016, **8**, 4762–4770.
32 H. Xuan, Y. Guan, X. Han, X. Liang, Z. Xie, P. Hanand Y. Wu, *Electrochim. Acta*, 2020, **335**, 135691.
33 Z. Hou, C. Shu, P. Hei, T. Yang, R. Zheng, Z. Ran, M. Liand J. Long, *Nanoscale*, 2020, **12**, 1864–1874.
34 J. Sun, P. Zan, L. Ye, X. Yangand L. Zhao, *J. Mater. Chem. A*, 2017, **5**, 9815–9823.
35 A. S. Arico, P. Bruce, B. Scrosati, J. M. Tarasconand W. Van Schalkwijk, *Nat. Mater.*, 2005, **4**, 366–377.
36 V. Augustyn, P. Simonand B. Dunn, *Energy Environ. Sci.*, 2014, **7**, 1597–1614.
37 M. Chen, Y. G. Zhang, L. D. Xing, Y. H. Liao, Y. C. Qiu, S. H. Yangand W. S. Li, *Adv. Mater.*, 2017, **29**, 1607015.
38 S. Liu, K. S. Hui, K. N. Hui, J. M. Yunand K. H. Kim, *J. Mater. Chem. A*, 2016, **4**, 8061–8071.
39 C. Choi, D. S. Ashby, D. M. Butts, R. H. DeBlock, Q. L. Wei, J. Lauand B. Dunn, *Nat. Rev. Mater.*, 2020, **5**, 5–19.
40 Q. B. Zhang, Z. C. Liu, B. T. Zhao, Y. Cheng, L. Zhang, H. H. Wu, M. S. Wang, S. G. Dai, K. L. Zhang, D. Ding, Y. P. Wuand M. L. Liu, *Energy Storage Mater.*, 2019, **16**, 632–645.
41 Y. Huang, L. Quan, T. Liu, Q. Chen, D. Caiand H. Zhan, *Nanoscale*, 2018, **10**, 14171–14181.
42 R. A. Patil, C. P. Chang, R. S. Devan, Y. Liouand Y. R. Ma, *ACS Appl. Mater. Interfaces*, 2016, **8**, 9872–9880.
43 J. Lin, H. Jia, H. Liang, S. Chen, Y. Cai, J. Qi, C. Qu, J. Cao, W. Feiand J. Feng, *Adv. Sci.*, 2018, **5**, 1700687.
44 F. Y. Ning, M. F. Shao, C. L. Zhang, S. M. Xu, M. Weiand X. Duan, *Nano Energy*, 2014, **7**, 134–142.
45 Y. Zhao, H. Dong, X. He, J. Yu, R. Chen, Q. Liu, J. Liu, H. Zhang, R. Liand J. Wang, *J. Power Sources*, 2019, **438**, 227057.
46 K. Wasinski, M. Walkowiak, P. Polrolniczakand G. Lota, *J. Power Sources*, 2015, **293**, 42–50.
47 S. Sun, T. Zhai, C. Liang, S. V. Savilovand H. Xia, *Nano Energy*, 2018, **45**, 390–397.

48 Y. Y. Ding, S. C. Tang, R. B. Han, S. Zhang, G. J. Panand and X. K. Meng, *Sci. Rep.*, 2020, **10**, 11023.
49 O. Ghodbane, J. L. Pascaland and F. Favier, *ACS Appl. Mater. Interfaces*, 2009, **1**, 1130–1139.
50 J. Xu, Y. Sun, M. Lu, L. Wang, J. Zhang, J. Qianand and X. Liu, *Chem. Eng. J.*, 2018, **334**, 1466–1476.
51 Z. S. Wu, G. M. Zhou, L. C. Yin, W. Ren, F. Liand and H. M. Cheng, *Nano Energy*, 2012, **1**, 107–131.
52 B. Y. Guan, L. Yu, X. Wang, S. Songand and X. W. Lou, *Adv. Mater.*, 2017, **29**, 1605051.
53 T. Kavinkumar, K. Vinodgopaland and B. Neppolian, *Appl. Surf. Sci.*, 2020, **513**, 145781.
54 N. Tuyenand and M. d. F. Montemor, *Adv. Sci.*, 2019, **6**, 1801797.
55 T. Zhai, S. Sun, X. Liu, C. Liang, G. Wangand and H. Xia, *Adv. Mater.*, 2018, **30**, 1706640.
56 J. Zhu, S. C. Tang, H. Xie, Y. M. Daiand and X. K. Meng, *ACS Appl. Mater. Interfaces*, 2014, **6**, 17637–17646.
57 Q. Yang, Z. Li, R. Zhang, L. Zhou, M. Shaoand and M. Wei, *Nano Energy*, 2017, **41**, 408–416.
58 S. R. Ede, S. Anantharaj, K. T. Kumaran, S. Mishraand and S. Kundu, *RSC Adv.*, 2017, **7**, 5898–5911.
59 X. Dai, D. Chen, H. Fan, Y. Zhong, L. Chang, H. Shao, J. Wang, J. Zhangand and C.-N. Cao, *Electrochim. Acta*, 2015, **154**, 128–135.
60 M. J. Cui, S. C. Tang, Y. J. Ma, X. L. Shi, J. A. Syedand and X. K. Meng, *J. Power Sources*, 2018, **396**, 483–490.
61 V. C. Boseand and V. Biju, *Bull. Mater. Sci.*, 2015, **38**, 865–873.
62 M. A. Woo, M.-S. Song, T. W. Kim, I. Y. Kim, J.-Y. Ju, Y. S. Lee, S. J. Kim, J.-H. Choyand and S.-J. Hwang, *J. Mater. Chem. A*, 2011, **21**, 4286–4292.
63 X. Zhao, F. Li, B. Li, T. Zhang, Q. Teng, L. Wang, H. Wangand and Y. Zhang, *J. Phys. Chem. Solids*, 2018, **113**, 134–141.
64 Y. C. Qiu, Y. H. Zhao, X. W. Yang, W. F. Li, Z. H. Wei, J. W. Xiao, S. F. Leung, Q. F. Lin, H. K. Wu, Y. G. Zhang, Z. Y. Fanand and S. H. Yang, *Nanoscale*, 2014, **6**, 3626–3631.
65 T. Y. Liu, Z. P. Zhou, Y. C. Guo, D. Guoand and G. L. Liu, *Nat. Commun.*, 2019, **10**, 675.
66 B. Liu, B. Y. Liu, Q. F. Wang, X. F. Wang, Q. Y. Xiang, D. Chenand and G. Z. Shen, *ACS Appl. Mater. Interfaces*, 2013, **5**, 10011–10017.
67 P. Ren, Z. Wang, B. Liu, Y. Lu, Z. Jin, L. Zhang, L. Li, X. Liand and C. Wang, *J. Alloys Compd.*, 2020, **812**, 152014.
68 Q. W. Zhou, J. C. Xing, Y. F. Gao, X. J. Lv, Y. M. He, Z. H. Guoand and Y. M. Li, *ACS Appl. Mater. Interfaces*, 2014, **6**, 11394–11402.
69 X. Gao, J. Bi, W. Wang, H. Liu, Y. Chen, X. Hao, X. Sunand and R. Liu, *J. Alloys Compd.*, 2020, **826**, 154088.
70 R. Yi, R. Wang, J. Duan, Z. Fang, H. Li, Z. Chen, A. Zhouand and Y. Sun, *Electrochim. Acta*, 2020, **338**, 135845.
71 X. J. Hou, X. F. Wang, B. Liu, Q. F. Wang, T. Luo, D. Chenand and G. Z. Shen, *Nanoscale*, 2014, **6**, 8858–8864.
72 F. H. Hsu, S. Y. Hsu, C. W. Pao, J. L. Chen, C. L. Chen, J. M. Chenand and K. T. Lu, *Nanoscale*, 2020, **12**, 13388–13397.
73 H. Tong, Q. Meng, J. Liu, T. Li, D. Gong, J. Xiao, L. Shen, T. Zhang, D. Bingand and X. Zhang, *J. Alloys Compd.*, 2020, **822**, 153689.
74 C. Zhang, Z. Xie, W. Yang, Y. Liang, D. Meng, X. He, P. Liangand and Z. Zhang, *J. Power Sources*, 2020, **451**, 227761.
75 A. Pendashteh, M. S. Rahmanifar, R. B. Kanerand and M. F. Mousavi, *Chem. Commun.*, 2014, **50**, 1972–1975.
76 Q. W. Zhou, J. C. Xing, Y. F. Gao, X. J. Lv, Y. M. He, Z. H. Guoand and Y. M. Li, *ACS Appl. Mater. Interfaces*, 2014, **6**, 11394–11402.
77 M. Sethi, U. S. Shenoyand and D. K. Bhat, *Nanoscale Adv.*, 2020, **2**, 4229–4241.
78 X. X. Zhu, M. Y. Sun, R. Zhao, Y. Q. Li, B. Zhang, Y. L. Zhang, X. Y. Lang, Y. F. Zhu and Q. Jiang, *Nanoscale Adv.*, 2020, **2**, 2785–2791.
79 A. A. Ensafi, S. E. Moosavifard, B. Rezaeiand and S. K. Kaverlavani, *J. Mater. Chem. A*, 2018, **6**, 10497–10506.
80 A. Mohammadi, N. Arsalani, A. G. Tabrizi, S. E. Moosavifard, Z. Naqshbandiand and L. S. Ghadimi, *Chem. Eng. J.*, 2018, **334**, 66–80.
81 B. Q. Xie, M. Y. Yu, L. H. Lu, H. Z. Feng, Y. Yang, Y. Chen, H. D. Cui, R. B. Xiaoand and J. Liu, *Carbon*, 2019, **141**, 134–142.
82 J. S. Sanchez, A. Pendashteh, J. Palma, M. Andersonand and R. Marcilla, *J. Mater. Chem. A*, 2019, **7**, 20414–20424.
83 W. Lu, M. Yang, X. Jiang, Y. Yu, X. Liuand and Y. Xing, *Chem. Eng. J.*, 2020, **382**, 122943.
84 H. Tong, W. Bai, S. Yue, Z. Gao, L. Lu, L. Shen, S. Dong, J. Zhu, J. Heand and X. Zhang, *J. Mater. Chem. A*, 2016, **4**, 11256–11263.
85 M. S. Javed, J. Chen, L. Chen, Y. Xi, C. Zhang, B. Wanand and C. Hu, *J. Mater. Chem. A*, 2016, **4**, 667–674.
86 J. Yang, Y. Zhang, C. Sun, G. Guo, W. Sun, W. Huang, Q. Yanand and X. Dong, *J. Mater. Chem. A*, 2015, **3**, 11462–11470.
87 Y. Chen, C. Jing, X. Fu, M. Shen, K. Li, X. Liu, H.-C. Yao, Y. Zhangand and K. X. Yao, *Chem. Eng. J.*, 2020, **384**, 123367.
88 K. V. G. Raghavendra, C. V. V. M. Gopi, R. Vinodh, S. S. Rao, I. M. Obaidatand and H.-J. Kim, *J. Energy Storage*, 2020, **27**, 101159.
89 A. Ray, A. Roy, M. Ghosh, J. Alberto Ramos-Ramon, S. Saha, U. Pal, S. K. Bhattacharyaand and S. Das, *Appl. Surf. Sci.*, 2019, **463**, 513–525.
90 V. K. Mariappan, K. Krishnamoorthy, P. Pazhamalai, S. Sahoo, S. S. Nardekarand and S.-J. Kim, *Nano Energy*, 2019, **57**, 307–316.
91 S. E. Moosavifard, S. Faniand and M. Rahmanian, *Chem. Commun.*, 2016, **52**, 4517–4520.
92 Y. M. Chen, Z. Liand and X. W. Lou, *Angew. Chem., Int. Ed.*, 2015, **54**, 10521–10524.
93 J. Xiao, L. Wan, S. Yang, F. Xiaoand and S. Wang, *Nano Lett.*, 2014, **14**, 831–838.
94 M. Liang, M. Zhao, H. Wang, J. Shenand and X. Song, *J. Mater. Chem. A*, 2018, **6**, 2482–2493.
95 Q. Yang, Y. Liu, M. Yan, Y. Leiand and W. Shi, *Chem. Eng. J.*, 2019, **370**, 666–676.

96 L. Abbasi, M. Arvandand and S. E. Moosavifard, *Carbon*, 2020, **161**, 299–308.
97 Y. D. Yin, R. M. Rioux, C. K. Erdonmez, S. Hughes, G. A. Somorjaiand and A. P. Alivisatos, *Science*, 2004, **304**, 711–714.
98 J. Wu, X. Shi, W. Song, H. Ren, C. Tan, S. Tangand and X. Meng, *Nano Energy*, 2018, **45**, 439–447.
99 J. Yang, C. Yu, X. Fan, S. Liang, S. Li, H. Huang, Z. Ling, C. Haoand and J. Qiu, *Energy Environ. Sci.*, 2016, **9**, 1299–1307.
100 Y. Li, H. Gao, Z. Sun, Q. Li, Y. Xu, C. Geand and Y. Cao, *J. Solid State Electrochem.*, 2018, **22**, 3197–3207.
101 Y. Zhu, S. An, X. Sun, D. Lan, J. Cui, Y. Zhangand and W. He, *Chem. Eng. J.*, 2020, **383**, 123206.
102 T. Tang, S. Cui, W. Chen, H. Houand and L. Mi, *Nanoscale*, 2019, **11**, 1728–1736.
103 W. He, C. Wang, H. Li, X. Deng, X. Xuand and T. Zhai, *Adv. Energy Mater.*, 2017, **7**, 1700983.
104 L. Hou, Y. Shi, S. Zhu, M. Rehan, G. Pang, X. Zhangand and C. Yuan, *J. Mater. Chem. A*, 2017, **5**, 133–144.
105 G. He, M. Qiao, W. Li, Y. Lu, T. Zhao, R. Zou, B. Li, J. A. Darr, J. Hu, M.-M. Titiriciand and I. P. Parkin, *Adv. Sci.*, 2017, **4**, 1600214.
106 J. A. Syed, J. Ma, B. Zhu, S. Tangand and X. Meng, *Adv. Energy Mater.*, 2017, **7**, 1701228.
107 T. Dang, D. Wei, G. Zhang, L. Wang, Q. Li, H. Liu, Z. Cao, G. Zhangand and H. Duan, *Electrochim. Acta*, 2020, **341**, 135988.
108 G. Qu, C. Li, P. Hou, G. Zhao, X. Wang, X. Zhangand and X. Xu, *Nanoscale*, 2020, **12**, 4686–4694.
109 H. Wang, Y. Zhu, Q. Zong, Q. Wang, H. Yangand and Q. Zhang, *Electrochim. Acta*, 2019, **321**, 134746.
110 Y. Lin, K. Sun, S. Liu, X. Chen, Y. Cheng, W.-C. Cheong, Z. Chen, L. Zheng, J. Zhang, X. Li, Y. Panand and C. Chen, *Adv. Energy Mater.*, 2019, **9**, 1901213.
111 X. Chen, M. Cheng, D. Chenand and R. Wang, *ACS Appl. Mater. Interfaces*, 2016, **8**, 3892–3900.
112 X. Li, H. Wu, A. M. Elshahawy, L. Wang, S. J. Pennycook, C. Guanand and J. Wang, *Adv. Funct. Mater.*, 2018, **28**, 1800036.
113 E. Hu, Y. Feng, J. Nai, D. Zhao, Y. Huand and X. W. Lou, *Energy Environ. Sci.*, 2018, **11**, 872–880.
114 H. Liang, C. Xia, Q. Jiang, A. N. Gandi, U. Schwingenschlogland and H. N. Alshareef, *Nano Energy*, 2017, **35**, 331–340.
115 K. Zhou, W. Zhou, L. Yang, J. Lu, S. Cheng, W. Mai, Z. Tang, L. Liand and S. Chen, *Adv. Funct. Mater.*, 2015, **25**, 7530–7538.
116 D. Khang Ngoc, Q. Liang, C.-F. Du, J. Zhao, A. L. Y. Tok, H. Maoand and Q. Yan, *Nano Today*, 2019, **25**, 99–121.
117 Y. Lan, H. Zhao, Y. Zong, X. Li, Y. Sun, J. Feng, Y. Wang, X. Zhengand and Y. Du, *Nanoscale*, 2018, **10**, 11775–11781.
118 N. Zhang, Y. Li, J. Xu, J. Li, B. Wei, Y. Ding, I. Arnorim, R. Thomas, S. M. Thalluri, Y. Liu, G. Yuand and L. Liu, *ACS Nano*, 2019, **13**, 10612–10621.
119 H. Wan, L. Li, Y. Chen, J. Gong, M. Duan, C. Liu, J. Zhangand and H. Wang, *Electrochim. Acta*, 2017, **229**, 380–386.
120 Z. Zhang, S. Liu, J. Xiaoand and S. Wang, *J. Mater. Chem. A*, 2016, **4**, 9691–9699.
121 Y.-M. Hu, M.-C. Liu, Y.-X. Hu, Q.-Q. Yang, L.-B. Kongand and L. Kang, *Electrochim. Acta*, 2016, **215**, 114–125.
122 X. Li, R. Ding, W. Shi, Q. Xu, L. Wang, H. Jiang, Z. Yangand and E. Liu, *Mater. Lett.*, 2017, **187**, 144–147.
123 Y. Huang, C. Chen, C. An, C. Xu, Y. Xu, Y. Wang, L. Jiaoand and H. Yuan, *Electrochim. Acta*, 2014, **145**, 34–39.
124 W. Song, J. Wu, G. Wang, S. Tang, G. Chen, M. Cuiand and X. Meng, *Adv. Funct. Mater.*, 2018, **28**, 1804620.

